THE ASTROPHYSICAL JOURNAL, 466:998–1010, 1996 August 1

HUBBLE SPACE TELESCOPE SPECTROSCOPIC OBSERVATIONS OF THE EJECTA OF SN 1987A AT 2000 DAYS[1]

LIFAN WANG[2] AND J. CRAIG WHEELER
Department of Astronomy and McDonald Observatory, The University of Texas at Austin, Austin, TX 78712;
lifan@astro.as.utexas.edu, wheel@astro.as.utexas.edu

ROBERT P. KIRSHNER AND PETER M. CHALLIS
Harvard-Smithsonian Center for Astrophysics, 60 Garden Street, MS-19, Cambridge, MA 02138

ALEXEI V. FILIPPENKO
Department of Astronomy, University of California, Berkeley, CA 94720

CLAES FRANSSON
Stockholm Observatory, S-133 00 Saltsjöbaden, Sweden

NINO PANAGIA[3]
Space Telescope Science Institute, 3700 San Martin Drive, Baltimore, MD 21218

AND

MARK M. PHILLIPS AND NICHOLAS SUNTZEFF
Cerro Tololo Inter-American Observatory, National Optical Astronomy Observatories, Casilla 603, La Serena, Chile
Received 1995 October 24; accepted 1996 March 6

ABSTRACT

We have used the Faint Object Spectrograph on the *Hubble Space Telescope* (*HST*) to observe the spectra of SN 1987A over the wavelength range 2000–8000 Å on dates 1862 and 2210 days after the supernova outburst. Even these pre-COSTAR observations avoid much of the contamination from the bright stars nearby and provide a very useful set of line strengths and shapes for analysis. The spectrum is formed in an unusual physical setting: cold gas that is excited and ionized by energetic electrons from the radioactive debris of the supernova explosion. The spectra of SN 1987A at this phase are surprisingly similar to those of the nova shells of CP Puppis and T Pyxidis decades after outburst. SN 1987A and the novae are characterized by emission from material with electron temperatures of only a few hundred kelvins and show narrow Balmer continuum emission and strong emission lines from O^+. The Balmer continuum shape requires the electron temperature in the supernova ejecta to be as low as 500 K on day 1862 and 400 K on day 2210 after outburst. The [O II] $\lambda\lambda$3726, 3728 doublet is surprisingly strong and is plausibly powered by collisional ionization of neutral oxygen to excited states of O^+.

The line intensity ratio of the [O I] $\lambda\lambda$6300, 6364 doublet obtained from Gaussian fits of the line profiles is 1.8 ± 0.2, contrary to the optically thin limit of 3. This ratio is *not* due to an optical depth effect but, rather, is an artifact of assuming a Gaussian profile to fit the [O I] $\lambda\lambda$6300, 6364 doublet profile. Specifying the line ratio $R = F([\mathrm{O\ I}]\ \lambda 6300)/F([\mathrm{O\ I}]\ \lambda 6364) = 3$ is consistent with the data and allows a calculation of the decomposed line profile.

All the observed strong lines are found to be blueshifted by a similar amount of 400 km s^{-1}. The line profiles are quite similar for lines arising from different chemical elements. The profiles are all asymmetric, showing redshifted extended tails with velocities up to 10,000 km s^{-1} in some strong lines. The blueshift of the line peaks is attributed to dust that condensed from the SN 1987A ejecta that is still distributed in dense opaque clumps. The strongest ultraviolet lines are those of Mg I λ2852 and Mg II $\lambda\lambda$2795, 2802. The Mg I λ2852 line is significantly broader than most lines in the optical, which provides a natural explanation for the size differences in the optical and ultraviolet of the SN 1987A ejecta derived from *HST* direct images.

Subject headings: stars: individual (SN 1987A) — supernova remnants — ultraviolet: stars

1. INTRODUCTION

SN 1987A provides a unique opportunity to observe the debris from a supernova explosion. As part of our Supernova INtensive Study (SINS) of supernovae with the *Hubble Space Telescope* (*HST*), we present spectroscopic observations obtained with *HST*. When these *HST* observations were taken, in 1992 and 1993, the ejecta were so cold that thermal electrons played a negligible role in the formation of optical and ultraviolet lines. The observed emission lines are powered through nonthermal excitations by fast electrons produced by collisions with the gamma rays that result from the decay of radioactive ^{57}Co and ^{44}Ti produced in the supernova explosion. Detailed models for the spectroscopic evolution of supernova ejecta in the nebular phase have been presented by several groups (Fransson & Chevalier 1989; Swartz 1991; Xu & McCray 1991; Kozma & Fransson 1992; Li & McCray 1995). An updated review paper is given by McCray (1993). The basic mechanism involves energy deposition by gamma rays from

[1] Based on observations with the NASA/ESA *Hubble Space Telescope*, obtained at the Space Telescope Science Institute, which is operated by AURA, inc., under NASA contract NAS 5-26555.
[2] Also Beijing Astronomical Observatory, Beijing 100080, P.R. China.
[3] Affiliated to the Astrophysics Division, Space Science Department of ESA.

radioactive materials (^{56,57}Co and ^{44}Ti) in the supernova ejecta. The fast electrons produce heating, excitation, and ionization. Five years after the supernova explosion, excitation and ionization dominate the energetics, while heating becomes unimportant because of the low ionization fraction of the ejecta. For most ions, recombination timescales in the SN 1987A ejecta at late times may exceed the dynamical and radioactive decay timescale, and the ionization stage of the ejecta will freeze out (Clayton, Leising, & The 1992; Fransson & Kozma 1993). As a result, emission lines from radiative recombination remain strong long after the supernova outburst. Late-time observations of SN 1987A provide us with an excellent opportunity to test these theories and to analyze the ejecta.

The purpose of this paper is to present the pre-COSTAR *HST* observations of SN 1987A, to present plausible explanations of the physical processes, and to derive some properties of the underlying event. We discuss in § 2 the observations and data reduction. The results from this study are given in § 3, where we discuss emission lines arising from hydrogen, oxygen, magnesium, and iron, and the properties of the dust in SN 1987A. We give conclusions from this study in § 4.

2. OBSERVATIONS AND DATA REDUCTION

The spectra of SN 1987A were acquired using the *HST* as part of the SINS). Observations with the Faint Object Spetrograph (FOS) were obtained on 1992 March 31, 1993 March 14, and 1993 April 1–6. Post-COSTAR observations were made on 1995 January 7 and will be the subject of a subsequent paper. In addition to these spectroscopic observations, there are also WFPC images taken as part of the same project. The direct images have been discussed by Plait et al. (1994) and by Pun et al. (1996). This paper concentrates on the two pre-COSTAR spectra.

The data were reduced using the standard *HST* postprocessing software. The pipeline-calibrated data were reduced with the most current calibration reference files. Table 1 contains the summary of the observations including data set name, date of observation, detector, grating, and exposure time. Table 2 contains the observational parameters including wavelength coverage, resolution, and dispersion. All the data were taken through the 0.″25 × 2.″0 slit. The slit was located to observe both the broad lines from the debris and narrow lines from the circumstellar ring simultaneously. Figure 1 shows the slit orientation and position for each set of observations. Both the 1992 March 31 and 1993 March 14 observations were centered on the debris. Figure 1 was created from a Faint Object Camera (FOC) observation of SN 1987A on 1992 April 12. The 1993 April 1–6 observations were not centered on the target; our best estimate is that the slit was positioned ~0.″3 east of the debris. These miscentered observations show spectral features of the circumstellar ring but no features from the debris. A new acquisition strategy has since been implemented to ensure the aperture is well centered on SN 1987A.

At the off-axis location of the FOS, the width (FWZI) of the point-spread function (PSF) of the optical system is about 2″–3″. Figure 1 shows that the light from star 3 (1.″3 away) overlaps the position of the FOS aperture. Since star 3 is a Be star (Wang et al. 1992; Walborn et al. 1993), the contamination is most serious in the UV. The amount of star 3 light in the supernova spectra can be estimated by two methods. First, the FOC images can be used to determine how much of the star 3 light enters the FOS aperture.

TABLE 1

SUMMARY OF FOS OBSERVATIONS OF SN 1987A

Data Set	UT Date (mm dd yy)	Grating	Detector	Exposure	Position
Y0WY0202T.....	03 30 92	FOS/RD	G400H	1500.0	Centered
Y0WY0203T.....	03 30 92	FOS/RD	G570H	1500.0	Centered
Y0WY0204T.....	03 31 92	FOS/RD	G780H	1500.0	Centered
Y0WY0102T.....	04 01 92	FOS/BL	G130H	1500.0	Centered
Y0WY0103T.....	04 02 92	FOS/BL	G130H	1500.0	Centered
Y0WY0104T.....	04 02 92	FOS/RD	G190H	1500.0	Centered
Y0WY0105T.....	04 02 92	FOS/RD	G190H	1500.0	Centered
Y0WY0106T.....	04 02 92	FOS/RD	G270H	1500.0	Centered
Y0WY0107T.....	04 02 92	FOS/RD	G270H	1500.0	Centered
Y0WY0602T.....	03 14 93	FOS/RD	G400H	1500.0	Centered
Y0WY0603T.....	03 14 93	FOS/RD	G570H	1500.0	Centered
Y0WY0604T.....	03 14 93	FOS/RD	G780H	1500.0	Centered
Y0WY5602T.....	04 01 93	FOS/RD	G400H	1500.0	Off-center
Y0WY5603T.....	04/01/93	FOS/RD	G570H	1500.0	Off-center
Y0WY5604T.....	04/01/93	FOS/RD	G780H	1500.0	Off-center
Y0WY0302T.....	04 02 93	FOS/BL	G130H	1500.0	Off-center
Y0WY0303T.....	04 02 93	FOS/BL	G130H	1500.0	Off-center
Y0WY0304T.....	04 02 93	FOS/RD	G190H	1500.0	Off-center
Y0WY0305T.....	04 02 93	FOS/RD	G190H	1500.0	Off-center
Y0WY0306T.....	04 02 93	FOS/RD	G270H	1500.0	Off-center
Y0WY0307T.....	04 02 93	FOS/RD	G270H	1500.0	Off-center
Y0WY0402T.....	04 03 93	FOS/RD	G400H	1500.0	Off-center
Y0WY0403T.....	04 03 93	FOS/RD	G570H	1500.0	Off-center
Y0WY0404T.....	04 03 93	FOS/RD	G780H	1500.0	Off-center
Y0WY0502T.....	04 06 93	FOS/BL	G130H	1500.0	Off-center
Y0WY0503T.....	04 06 93	FOS/BL	G130H	1500.0	Off-center
Y0WY0504T.....	04 06 93	FOS/RD	G190H	1500.0	Off-center
Y0WY0505T.....	04 06 93	FOS/RD	G190H	1500.0	Off-center
Y0WY0506T.....	04 06 93	FOS/RD	G270H	1500.0	Off-center
Y0WY0507T.....	04 06 93	FOS/RD	G270H	1500.0	Off-center

TABLE 2

OBSERVATIONAL PARAMETERS

FOS Grating	Detector	Wavelength Region (Å)	Dispersion (Å pixel^{-1})	Resolution (FWHM [Å])	Aperture (arcsec)
G130H.....	Blue	1140–1605	0.25	1.1	0.5 × 2.0
G190H.....	Red	1600–2310	0.36	1.5	0.25 × 2.0
G270H.....	Red	2230–3270	0.51	2.1	0.25 × 2.0
G400H.....	Red	3250–4791	0.74	3.1	0.25 × 2.0
G570H.....	Red	4200–6800	1.08	4.1	0.25 × 2.0
G780H.....	Red	6500–8600	1.43	5.1	0.25 × 2.0

Second, the FOS observations from 1995 January during the COSTAR era can be used as a guide to adjust the pre-COSTAR data. A correction can be calculated by measuring the difference in the flux level between the emission lines of the pre-COSTAR and the post-COSTAR spectra. Both methods give a consistent correction to the data. The contamination of the observed spectra by star 3 varies with wavelength and ranges from as large as 75% at 2000 Å to 17% at 4000 Å. At wavelengths longer than 5000 Å, this contamination is below 1%. The observations made with the blue side of G130H FOS are completely dominated by star 3 light. No emission features were detected from either the debris or the circumstellar ring.

3. RESULTS

The final flux-calibrated spectra are corrected for interstellar extinction assuming $E(B-V) = 0.2$ mag (Panagia et al. 1987) and $A_v = 0.62$. The spectra are shown in Figure 2 with the suggested line identifications. The original spectra consist of both narrow forbidden lines typical of H II regions and broad lines of FWHM greater than 2000 km s^{-1}. The narrow lines were first observed with the *IUE* (Fransson et al. 1989) in the ultraviolet about 80 days after the supernova explosion and from the ground (Wampler & Richichi 1989) in the optical about 300 days after the explosion. These lines are believed to be due to the circumstellar material in the immediate SN 1987A environment, presumably material lost by the progenitor's stellar winds. The broad lines are from the supernova debris itself and are the main topic of the current study. All the narrow lines have been removed from the spectra in Figure 2 but form the subject of a future paper (Panagia et al. 1996).

A complete list of the emission lines from the debris is given in Table 3. The wavelengths given in the table were approximate measured values of the line peaks. The line strengths were measured by fitting a simple Gaussian profile with a linear background. There are three main difficulties in measuring the line strengths. First, there are the

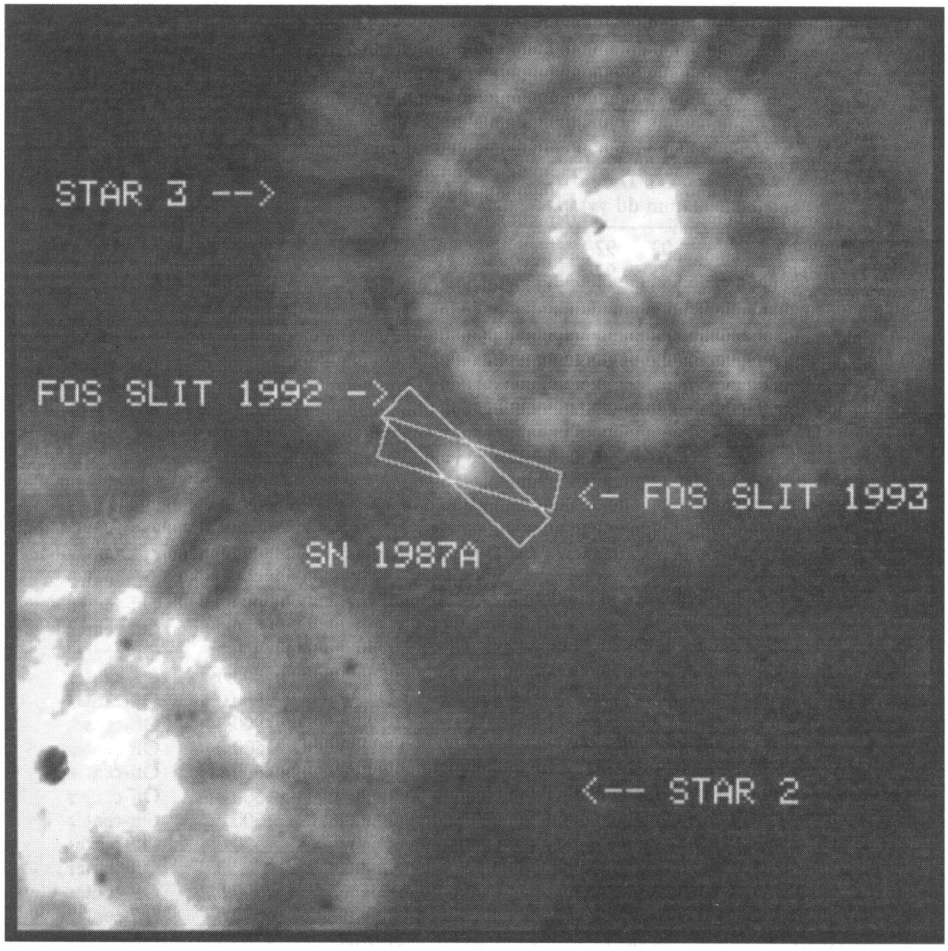

FIG. 1.—Slit orientation and position for each set of observations

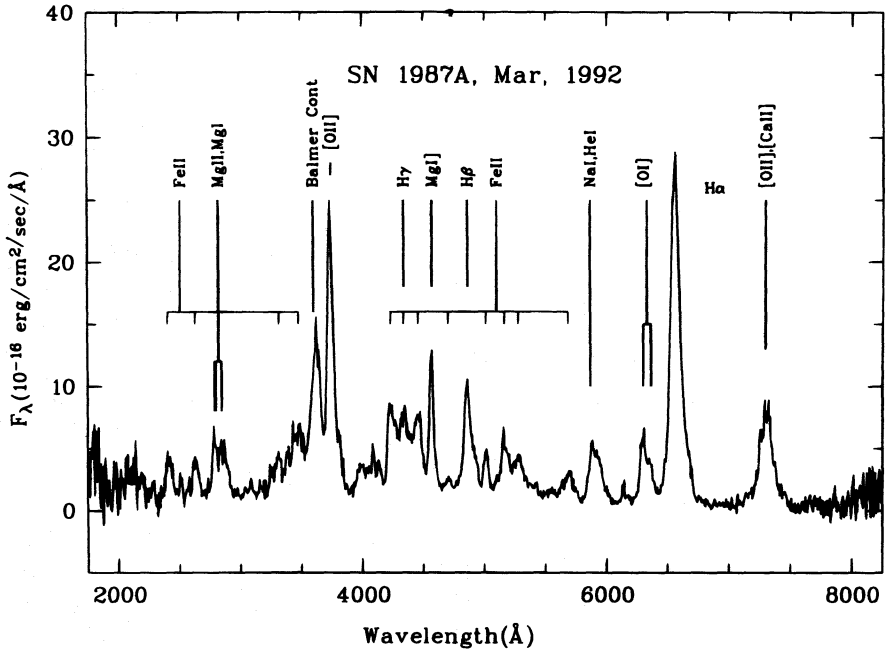

FIG. 2*a*

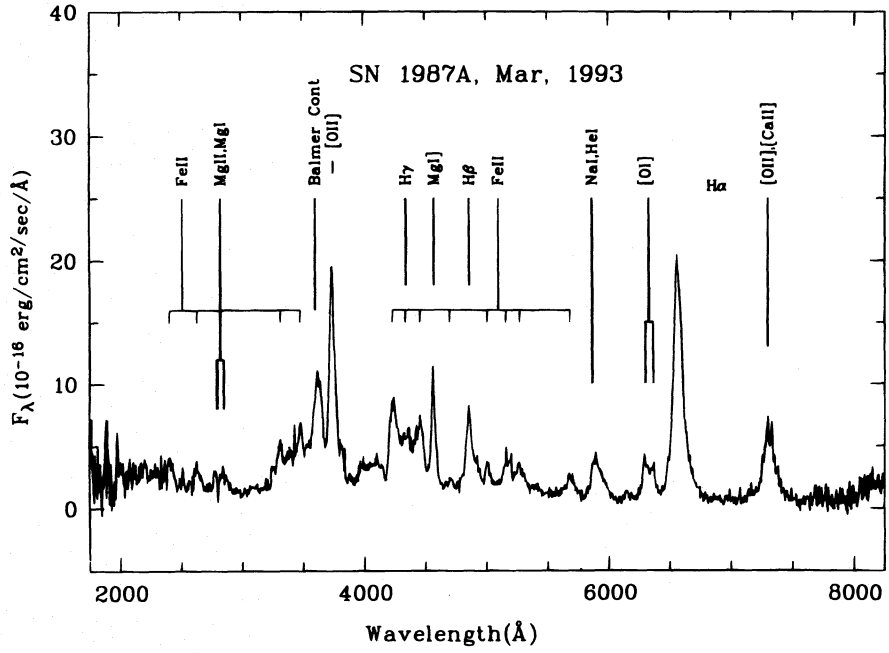

FIG. 2*b*

FIG. 2.—(*a*) The 1992 March 31 spectrum and the suggested line identifications; (*b*) the 1993 March 14 spectrum. Both spectra are corrected for interstellar extinction assuming $E(B-V) = 0.2$ mag. The circumstellar lines are removed from the spectra.

narrow emission features from the circumstellar ring blended with the broader debris lines. These emission features were fitted with a single Gaussian profile with a linear background and subtracted. Second, the debris emission features are not exactly Gaussian, as discussed in § 4. Line strengths obtained by simply integrating above a continuum are accurate to within this uncertainty, and therefore only values from Gaussian fits are tabulated. Third, the continuum level is often difficult to measure as many of the lines are blended. The estimate of the uncertainty of the line strength is 10%–20% including also the uncertainties in the calibration of the absolute flux level. However, the relative strengths of the lines are more reliable and are accurate to about 5%. The observed Hα fluxes are 1.66×10^{-13} ergs cm^{-2} s^{-1} Å^{-1} and 1.17×10^{-13} ergs cm^{-2} s^{-1} Å^{-1} for the 1992 and 1993 spectra, respectively. The dereddened Hα fluxes for the 1992 and 1993 spectra are 2.62×10^{-13} ergs cm^{-2} s^{-1} Å^{-1} and 1.84×10^{-13} ergs cm^{-2} s^{-1} Å^{-1}, respectively.

Most of the lines that appeared in earlier nebular phase spectra, such as those identified by Phillips & Williams (1991) and Kirshner et al. (1987), are still detectable. The strongest lines are Hα, Hβ, and [O I] λλ6300, 6364 in the optical and the resonance Mg I λ2852, Mg II λλ2795, 2802 lines discussed in detail by Pun et al. (1995) in the ultraviolet. A remarkable feature shown by the current data is that

TABLE 3

LINE LIST

WAVELENGTH (Å)	1992 MAR 30 Flux[a]	1992 MAR 30 Flux[b]	1992 MAR 30 FWHM (Å)	1993 MAR 14 Flux[a]	1993 MAR 14 Flux[b]	1993 MAR 14 FWHM (Å)	IDENTIFICATION
2410.3.....	2.6	6.8	58.7	2.0	5.0	60.2	Fe II (UV2)
2630.4.....	3.0	6.5	59.6	2.7	5.9	54.6	Fe II (UV1)
2828.8.....	10.5	20.6	135.0	6.4	12.7	127.3	Mg II λλ2795, 2802, Mg I UV
3314.5.....	1.8	3.1	50.0	2.4	4.1	45.0	Fe II (1)
3476.4.....	2.1	3.5	39.0	2.7	4.4	45.1	Fe II (4, 6), Fe I (6)
3620.5.....	18.4	29.7	79.5	15.2	24.6	72.1	Bac
3737.8.....	21.0	32.8	63.6	24.6	38.6	49.7	[O II] λλ3726, 3728
4229.3[c]							[Fe II] (21F)
4335.7[c]	41.4	55.9	282.1	50.4	68.0	284.0	Hγ, [Fe II] (21F)
4456.3[c]							[Fe II] (6F)
4554.3.....	13.5	17.4	41.3	13.9	18.0	39.3	Mg I] λ4571
4701.9.....	1.5	1.9	52.9	3.0	3.8	60.0	[Fe II] (5F)
4863.8.....	20.7	25.4	86.2	22.2	27.3	75.1	Hβ
5010.9.....	5.1	6.0	45.3	3.6	4.3	39.1	[Fe II] (4F)
5160.0.....	11.1	13.0	78.6	7.8	9.2	73.8	[Fe II] (18F, 35F)
5277.0.....	9.9	11.5	93.7	6.4	7.3	83.6	[Fe II] (17F, 18F, 35F)
5685.2.....	9.0	9.9	118.2	9.3	10.3	107.6	[Fe II] (33F)
5895.2.....	20.1	21.5	118.7	20.1	21.6	119.2	He I λ5876, Na I λ5896
6294.3.....	17.4	17.8	99.9	19.1	19.6	115.7	[O I] λλ6300, 6364
6558.8.....	100.0	100.0	97.1	100.0	100.0	96.0	Hα
7306.6.....	44.7	42.0	125.1	42.2	39.6	133.9	[O II] λ7320, [Ca II] λ7300

[a] Observed flux.
[b] Dereddened flux.
[c] These three lines are blended.

some of the iron lines, such as the [Fe II] λ7155 line, which were strong in the early spectra, have now disappeared. The temperature of the supernova ejecta is too low, and excitations by thermal electrons are no longer important for optical emission lines like [Fe II] λ7155 at this epoch. As a consequence, most of the thermally excited emission lines should appear in the infrared where thermal excitations are still important. This behavior is related to the so-called infrared catastrophe as studied in detail by Fransson & Chevalier (1989).

An interesting problem is that there are still several strong lines without secure identification, notably the emission features at wavelengths 3630 Å and 3727 Å. These lines will be discussed in more detail in the subsequent sections of this paper. We show that these are likely to be the Balmer continuum at low temperature and [O II] produced by ionization of neutral oxygen to excited states of O^+.

3.1. *Hydrogen Emission*

3.1.1. Hα *and* Hβ *Lines*

Hydrogen Balmer lines remain the strongest optical lines. The profiles of Hα and Hβ lines show an asymmetric redshifted tail out to 10,000 km s^{-1} for Hα and 7000 km s^{-1} for Hβ, beyond which the line profile is corrupted by an iron line. The profiles are shown in Figure 3 for the two epochs of observation. Both the Hα and Hβ profiles show the same asymmetry, so this is an intrinsic feature of the hydrogen, not a blending with other lines.

The asymmetric component in the line profile can be extracted by flipping the blue side of the Hα profile about the line peak and subtracting it from the red wing of the line profile. This results in a bump as broad as 8000 km s^{-1} (FWZI) centered at a redshift about 4000 km s^{-1}. The central velocity of this asymmetric component is in remarkable agreement with the analysis of the redshifted lines observed between day 200 and day 500 (Spyromilio, Meikle, & Allen 1990) and the red emission satellite of the hydrogen lines between day 20 and day 100, the asymmetry noted by Hanuschik & Dachs (1987), Larson et al. (1987), Phillips & Heathecote (1989), and Spyromilio et al. (1990). Chugai (1991a, 1991b) suggested that this asymmetric component is due to an asymmetric distribution of radioactive clumps in the SN 1987A ejecta.

3.1.2. *Hydrogen Balmer Continuum*

Another interesting feature is at wavelength 3630 Å. While this appears to be an emission line with width comparable to other lines, we identify it as hydrogen Balmer continuum emission, based on the argument developed by Williams (1982) in his spectroscopic analysis of the shells around novae. The nova shells Williams analyzed are quite cold, with electron temperature of only about 800 K. They emit unusual spectra in which recombination lines, including some forbidden lines formed by recombination, are quite strong. Because the emission coefficient for the Balmer continuum varies as $j_\nu \sim \exp[h(\nu_0 - \nu)/kT_e]$, where ν_0 is the Balmer ionization frequency, the Balmer continuum profile drops very sharply at frequencies higher than ν_0 when the kinetic temperature of the free electrons is very low, producing a narrow emission feature in the spectrum.

This identification of the Balmer continuum profile provides us with a powerful method for estimating the electron temperature in the ejecta. In order to do so, we have constructed a simple model that assumes that (1) there is a uniform distribution of hydrogen atoms inside a sphere of velocity smaller than 3000 km s^{-1}; (2) the temperature is constant across the entire nebula; and (3) the ejecta are optically thin to Balmer continuum photons. Assumption (1) is required mainly because of the lack of knowledge of the density structure of the debris; however, it is perhaps not very far from reality considering the complex chemical mixing processes indicated by various observations and

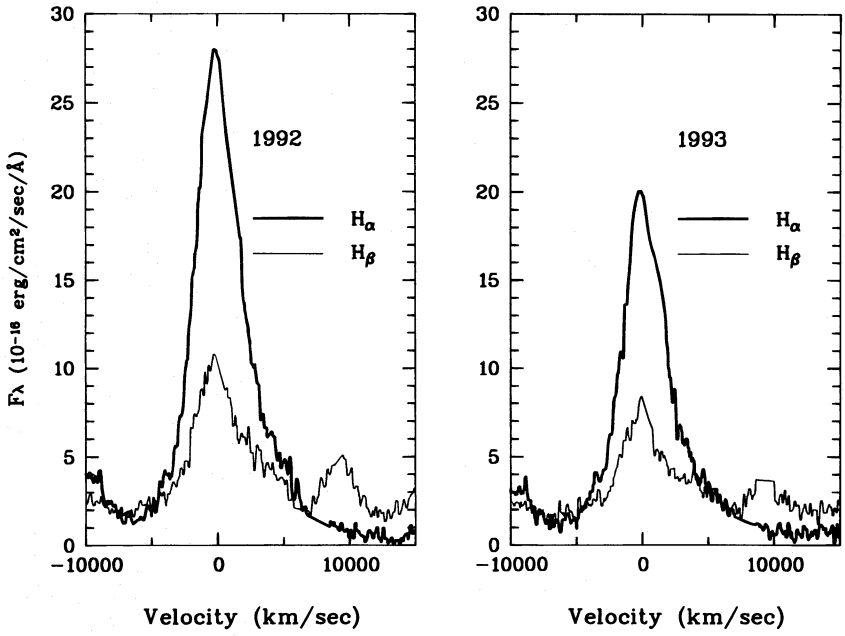

FIG. 3.—Hα and Hβ line profiles showing redshifted tails with velocities reaching 10,000 km s^{-1}. The Hβ line is apparently asymmetric, but the redshifted tail is corrupted by a neighboring iron line. Note that the narrow Hα, Hβ, and [N II] lines are removed.

models (see McCray 1993 for a review of this topic). Assumption (2) implies that the temperature to be deduced is only an average value. Assumption (3) can be justified because the ejecta are now much more extended than in early phases of evolution and are now transparent to Balmer continuum photons (see, e.g., McCray 1993).

The blue side of the Balmer continuum profile is temperature sensitive but is insensitive to the density structure. On the other hand, the redshifted portion of the Balmer continuum is determined primarily by the density structure of the ejecta, in which different velocities give different weights that alter the Doppler smearing of the Balmer edge. By matching both the blueshifted and redshifted parts of the profile, we are able to deduce the temperature of the ejecta quite accurately. The model profiles are plotted together with the observed line profiles in Figure 4. The corresponding best values of the electron temperature are 500 K on 1992 March 31 and 400 K on 1993 March 14. The uncertainties in these estimates are less than 100 K, and they result mainly from uncertainties in setting the underlying continuum level below the Balmer feature. The temperatures deduced are reliable for a wide range of possible density structures. Numerical experiments show that a uniform density sphere with radius at velocities ranging from 2500 to 4000 km s^{-1} provides satisfactory fits to both the 1992 March and 1993 March observations and yields practically the same electron temperatures for each epoch.

As an additional test of the identification of the 3630 Å, feature with the Balmer continuum profile, we have estimated the electron densities required to produce the observed total flux in the Balmer continuum. Adopting the same model parameters as used in deducing the line profiles, the average electron densities required are found to be $3.2 \times 10^3 (v/3000 \text{ km s}^{-1})^{-3/2}$ cm^{-3} and $2.5 \times 10^3 (v/3000 \text{ km s}^{-1})^{-3/2}$ cm^{-3} for the 1992 and 1993 data, respectively. For comparison, we can also derive electron densities using

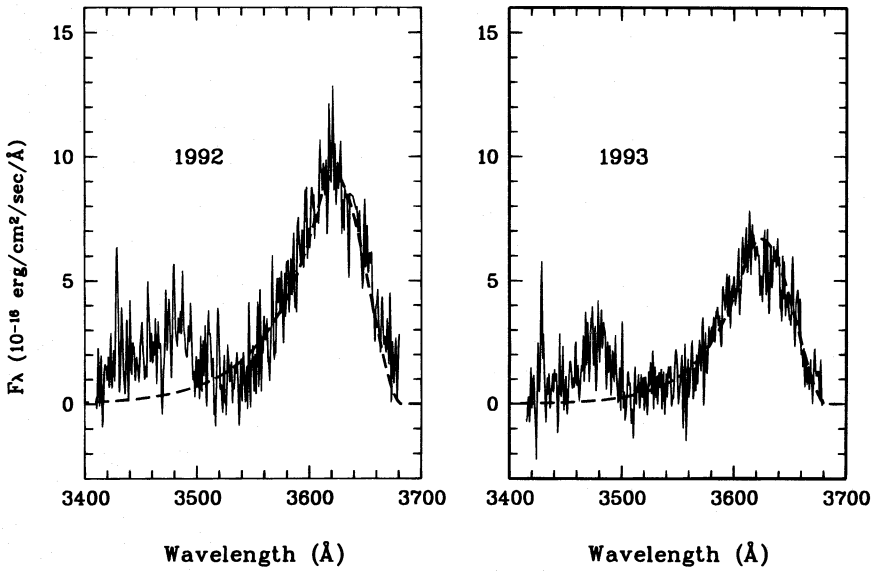

FIG. 4.—Observed hydrogen Balmer continuum profiles (*solid lines*) and the corresponding model fits (*dashed lines*)

the Hα line. Assuming that recombination of thermal electrons is the only process responsible for the Hα line, the electron density for both epochs is found to be $6.3 \times 10^3 (v/3000 \text{ km s}^{-1})^{-3/2} \text{ cm}^{-3}$ at day 1862. This is 2–3 times larger than the densities derived for the Balmer continuum. However, considering both the uncertainties in the absolute calibrations of the spectra and the oversimplified nature of the model, this agreement is satisfactory and adds to the evidence that our identification is correct. The derived electron density implies that the hydrogen-rich region is mostly neutral with ionization fraction around $1.2 \times 10^{-4} (M_H/10\,M_\odot)^{-1}$.

Chugai et al. (1993) reported identification of the Paschen continuum in the infrared and used the Paschen continuum to determine the temperature of the hydrogen emitting region. The redshifted part of the Paschen continuum is corrupted by some unidentified features, and the temperature determination is less accurate than that derived here from the Balmer continuum. Nonetheless, the temperatures obtained from the Paschen continuum are consistent with what we have derived in this study.

3.2. *Oxygen Lines*

3.2.1. [O I] λλ6300, 6364 *Doublet*

Chugai (1988) noted that in the case of supernova explosions, forbidden lines such as [O I] λλ6300, 6364 are optically thick for about one year after the explosion, due mainly to the high densities encountered. The doublet ratio $R = F([\text{O I}]\ \lambda 6300)/F([\text{O I}]\ \lambda 6364)$ will be smaller than its optically thin limit of 3. The ratio R can be used to estimate the average density of the oxygen-emitting region. Time evolution of the line ratio R was indeed observed by Phillips & Williams (1991) who found $R \approx 1$ at about 100 days after explosion increasing to about 2.6 at about 500 days after the explosion. Several authors have used this method to calculate the oxygen density in the SN 1987A ejecta (Spyromilio & Pinto 1991; Li & McCray 1992). The oxygen density derived from this method is $n_{\text{O I}} = 1.3 \times 10^9 t_y^{-3} \text{ cm}^{-3}$. This is too large if all the oxygen is distributed uniformly and suggests that most of the oxygen is in dense clumps with a volume-filling factor $f_O \approx 0.09 M_O/M_\odot$. Five years after the outburst, the density of the ejecta has greatly decreased, and the [O I] λλ6300, 6364 doublet should turn optically thin with a line ratio $R = 3$. However, the simple two-Gaussian profile fits yield a ratio $R = 1.9 \pm 0.1$ for both the 1992 and 1993 observations. This ratio is significantly different from the optically thin limit of 3 and is even smaller than the previously reported ratio of 2.6 on day 500 (Phillips & Williams 1991).

If we still apply Chugai's method for density determination, we would arrive at an oxygen density of $4.1 \times 10^8 \text{ cm}^{-3}$ on day 1862 and $3.7 \times 10^8 \text{ cm}^{-3}$ on day 2210. If the oxygen mass is of the order of 1–2 $M_\odot$ and if the majority of the oxygen mass is distributed inside a shell with maximum velocity of 1700 km s^{-1} (as used by Li & McCray 1992), a volume-filling factor of $\sim 2 \times 10^{-3}$ can be derived. This is about 2 orders of magnitude smaller than the value deduced by Li & McCray (1992) using the same lines but for early observations. The latter authors found a volume-filling factor of about 0.12 by modeling observations prior to day 500. Such a change could occur if the majority of the oxygen material is not emitting efficiently at late times, and only the densest parts of the ejecta are responsible for the observed line fluxes. In such a scenario, the early observations show the less dense part of the ejecta, while the later observations show the denser clumps of the ejecta which occupy less volume. This possibility, however, is unlikely as judged by the physical processes responsible for the line emission. The SN 1987A ejecta are expanding homologously, and the density should drop as t_y^{-3}. At such late stages of the supernova ejecta, as we have derived above from the Balmer continuum, the electron temperature is as low as several hundred kelvins. This means that thermal excitations are negligible in powering the emission lines, and the [O I] λλ6300, 6364 doublet photons are produced purely by nonthermal excitations by fast electrons from gamma-ray deposition in the ejecta. Since the ejecta are now optically thin to gamma rays, the energy deposited per atomic oxygen is nearly independent of local oxygen density. We would then expect that all oxygen atoms are excited equally; thus, it does not seem likely that only the densest part in the ejecta contributes to the [O I] λλ6300, 6364 emission. Another possibility is that the oxygen is becoming more clumpy with time, but this would require strong deviations from homologous expansion of the ejecta. No physical model leads naturally to this situation.

Blending with other lines may also be possible. Lines that are close to [O I] λ6364 include those from Fe I multiplet 13, forbidden transitions of Fe I mulitplet F17, Fe II multiplet 40, and Ti I multiplet 1. Line blending may affect the measured line ratio, but quantitative estimates of the effect are difficult. Here we restrict our analysis to contributions by a *single* third emission line having the same velocity structure as [O I] λλ6300, 6364. The observed line profiles are modeled by minimizing χ^2 fits of three Gaussians. We assume (1) all three Gaussians have the same FWHM; and (2) the contributions from [O I] λλ6300, 6364 are given by two Gaussians with intensity ratio of 3/1 of which the weaker component is redshifted by 3047.6 km s^{-1} (64 Å) with respect to the blue component. The approximate continuum level is simultaneously fitted by a linear function. Figure 5*a* shows the results of such experiments. The goodness of the fit is considerably improved compared with the two-Gaussian fit described above. The strengths of the postulated third component are 14.4% and 27.3% of the total line fluxes in the 1992 and 1993 spectra, respectively. The absolute strength and the profile of this component did not change during the two observations. The increase in its relative contribution to the total line intensity was due to a decrease in the total line intensity. The centroid of the third Gaussian is redshifted by 2500 ± 73 km s^{-1} (52 ± 1.5 Å) with respect to the [O I] λ6300 line. The iron line closest in wavelength is from Fe I λ6355.6 (multiplet 13). However, Fe I λ6355.6 should be blended with other Fe I multiplet 13 lines at wavelength 6402.1 Å, 6360.5 Å, and 6282.4 Å. Because the permitted Fe I lines can be optically thick at the time of the observations, these lines may be as strong as Fe I λ6355.6. The overall contribution from the Fe I multiplet 13 should thus have a profile very different from that of a single line. The lines of Fe II multiplet 40, and Ti I multiplet 1, although having acceptable wavelengths, may have the same difficulties in explaining the observed line ratio. An alternative explanation of the abnormal line ratio is that the [Fe II] λλ6340, 6444 (15F) line is strong in SN 1987A (J. Spyromilio 1995, private communication). The problem with this possibility is that the [Fe II] λ6444 line is usually stronger than the [Fe II] λ6340, and it is too far to the red side of the [O I] λ6364 line to fit the observations. Unless a

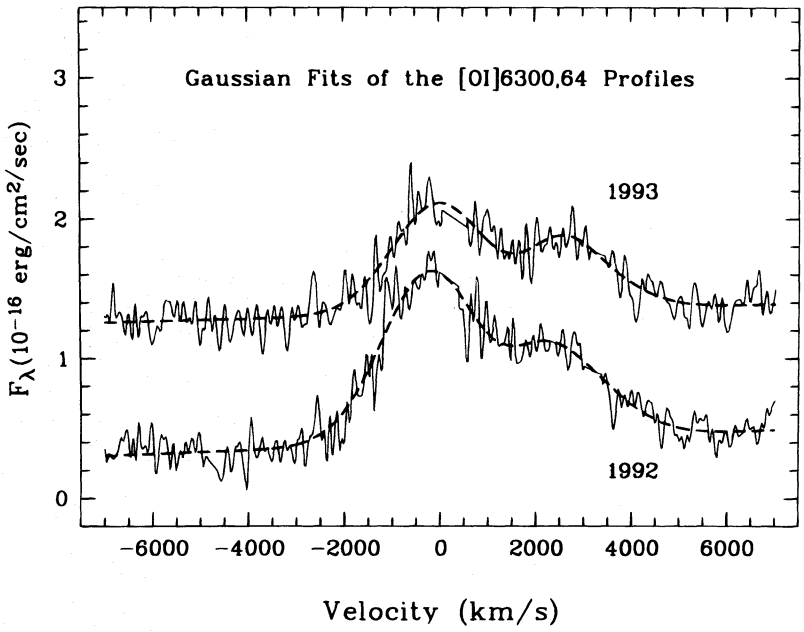

FIG. 5*a*

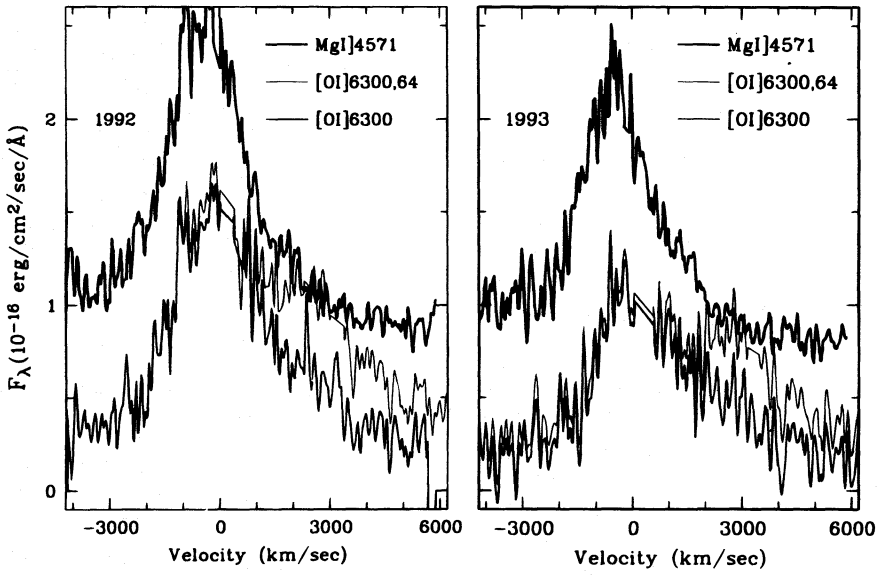

FIG. 5*b*

FIG. 5.—(*a*) The [O I] λλ6300, 6364 profiles and three-Gaussian fits. The parameters and constraints employed are given in the text. (*b*) The [O I] λλ6300, 6364 doublet decomposed by setting the ratio $R = 3$. The decomposed line profiles are compared with the profiles of the Mg I] λ4571 line for each observation. Note that the Mg I] λ4571 lines are arbitrarily shifted upwards for clarity. The sum of the [O I] λ6300 and [O I] λ6364 profiles matches exactly the corresponding observed [O I] λλ6300, 6364 profile by definition (see eq. [3]).

reliable model of the iron emission process is available, it is hard to analyze the iron lines quantitatively. Nevertheless, it seems difficult to account for the observed [O I] λλ6300, 6364 line ratio by contamination with a third component.

An alternative explanation is that the ratio deduced by line profile fitting is an artifact of the technique. In fact, by assuming different line profiles, one gets quite different values of the line ratios with satisfactory matches to the observed line profiles. A unique solution of the line ratio R is never guaranteed. To be more specific, the problem of the doublet decomposition is described by the following simple equation:

$$F(\lambda) = A_1(\lambda) + A_2(\lambda + \Delta\lambda_0)/R\ , \qquad (1)$$

where F is the flux of the [O I] λλ6300, 6364 doublet, λ is the wavelength, $\Delta\lambda_0$ is the wavelength difference of the two lines that is equal to 64 Å in the present case, and A_1 and A_2 are the line profiles for the 6300 Å and 6364 Å lines, respectively. We will assume that the [O I] λ6300 and [O I] λ6364 lines have the same line profile; A_1 and A_2 are then identical.

Instead of using Gaussian profiles to calculate the ratio R, we reverse the process by fixing the ratio R and calculating the resulting line profile A. This avoids the ambiguities of unknown line profiles and produces a clearer physical picture. In addition, the solution is mathematically unique for each value of R. We show in Figure 5*b* the decomposed profiles of the [O I] λ6300 and [O I] λ6364

lines together with the observed profile of the Mg I] λ4571 line for comparison, assuming a line ratio $R = 3$ for the [O I] doublet. It is surprising that such a simple technique yields [O I] λ6300 line profiles that are strikingly similar to those of the Mg I] λ4571 line. This agreement suggests that the decomposed profiles are adequate representations of each individual component of the [O I] λλ6300, 6364 doublet and argues strongly that the line ratio is in good agreement with the theoretical value expected in the optically thin limit, $R = 3$. Least χ^2 fit of the doublet ratio using the Mg I] λ4571 line as a template yields numbers of 3.1 ± 0.3 for the two epochs of observations. The uncertainties arise largely from the difficulties in defining the continuum level for the lines.

The present analysis shows that the line ratio depends sensitively on the assumed line profile. It raises doubts concerning the early [O I] λλ6300, 6364 doublet ratios derived by line profile fitting (Phillips & Williams 1991; Spyromilio & Pinto 1992). We believe that a more careful analysis of the early data, considering the approaches outlined above, is required before drawing quantitative conclusions about the oxygen density in the SN 1987A ejecta. A detailed comparison of the early optically thick oxygen profiles with the later optically thin profiles is of critical importance in establishing a quantitative picture of the oxygen-emitting region in the SN 1987A ejecta.

3.2.2. [O II] λλ3726, 3728

The prominent [O II] λλ3726, 3728 line requires some remarks. Surprisingly, this line is one of the strongest in the SN 1987A spectra—in fact, second only to Hα. As for the [O I] λλ6300, 6364 lines, the temperature of the ejecta is too low for thermal electrons to excite the [O II] λλ3726, 3728 doublet at the epochs of these observations, so only nonthermal excitations of the O^+ ions are important. The ionization fraction of the oxygen-rich region 5 years after explosion is less than 0.001 as shown by several calculations (Fransson & Chevalier 1989; Xu & McCray 1991; Kozma & Fransson 1992); therefore, only a minuscule fraction of the oxygen is ionized. Detailed calculations that take into account nonthermal excitations show that the expected [O II] λλ3726, 3728 doublet strength should be less than 10% of that of the [O I] λλ6300, 6364 lines (Kozma & Fransson 1992), while the observed line strength of [O II] λλ3726, 3728 is considerably larger than that of [O I] λλ6300, 6364.

As discussed by Williams (1982) in his explanation of the unusual spectra of the shells of novae, another way to produce the [O II] λλ3726, 3728 lines may be the recombination of O^{++} ions. The [O II] λλ3726, 3728 lines are the strongest optical recombination lines from O^{++}. However, taking the effective recombination rates for the [O II] λλ3726, 3728 doublet as given by Péquignot, Petitjean, & Boisson (1991), it is easy to verify that recombinations produce an insignificant amount of [O II] λλ3726, 3728 photons.

A more natural mechanism for powering the [O II] λλ3726, 3728 doublet is ionization of atomic oxygen directly to excited states of O^+ in a single impact. Updated excitation and ionization cross sections for electron impact on atomic oxygen by Laher & Gilmore (1989) include the cross sections of collisional ionization to excited states of O^+. Their results show that for electrons with energy above several tens of electron volts, a significant fraction of the ionizations of the neutral oxygen end up with O^+ ions in their $^2D^0$, $^2P^0$, and ^4P states. For example, when the energy of the free electron is 50 eV, about 20.6% of the total ionized O^+ ions go to the $^2D^0$ state, and 59.4% go to the ground state $^4S^0$; at very high energies (>1000 eV), the ionization to the ground state of the O^+ line is 36%, to $^2D^0$ is 30%, to $^2P^0$ is 17%, and to ^4P is 18%. The fractions going into excited states are almost independent of the energy of the free electrons at energies above 1000 eV.

The spontaneous decay of the levels $^2D^0$, $^2P^0$, and ^4P of O^+ can be an efficient route to produce [O II] λλ3726, 3728 and [O II] λλ7319, 7330 photons. The only path for the decay of $^2D^0$ is to the ground level with the emission of [O II] λλ3726, 3728. The $^2P^0$ level decays to the ground level producing [O II] λ2471 or to the $^2D^0$ level with the emission of [O II] λ7330, with a branching ratio of 0.3775. For each ionization of neutral oxygen, the number of [O II] λλ3726, 3728 photons produced is then

$$\xi = r_{^2D^0} + 0.3775 r_{^2P^0} , \tag{2}$$

where ξ is the fraction of ionizations to the excited states of O^+, and $r_{^2D^0}$ and $r_{^2P^0}$ are the fraction of ionizations to the states $^2D^0$ and $^2P^0$, respectively. Collisional de-excitation of the $^2D^0$ level can be important, further reducing the line flux approximately by a factor of $\eta = 1/(1 + N_e/N_{cr})$, where the critical density $N_{cr} = 3.6 \times 10^3$ cm^{-3} at a typical temperature of 500 K (Osterbrock 1989), and N_e is the electron density. The ionization of the neutral oxygen per second per cubic centimeter is

$$4\pi \frac{J_\gamma \sigma_{\gamma,\mathrm{O\,I}}}{\chi_{\mathrm{eff,O\,I}}} n_{\mathrm{O\,I}} \tag{3}$$

where J_γ is the mean gamma-ray intensity, and $\sigma_{\gamma,\mathrm{O\,I}} = \kappa_\gamma A_{\mathrm{O\,I}} m_p$ with the mass absorption coefficient $\kappa_\gamma = 0.06 Z_{\mathrm{O\,I}}/A_{\mathrm{O\,I}}$ cm^2 g^{-1}. Here $Z_{\mathrm{O\,I}} = 8$ and $A_{\mathrm{O\,I}} = 16$ are the atomic number and mass of the element.

For ionization fraction $x_e \ll 1$, the gamma-ray mean intensity is given by (Kozma & Fransson 1992)

$$J_\gamma = \frac{D_\gamma L_\gamma}{16\pi^2 (vt)^2} \tag{4}$$

where D_γ is a geometric factor of order unity, v is the velocity of the ejecta, and the luminosity of the gamma rays L_γ is given by

$$L_\gamma = 9.1 \times 10^{41} \left[\frac{M(^{56}\mathrm{Ni})}{0.07\, M_\odot}\right] (e^{-t/111.3} + 9.3 \times 10^{-4} e^{-t/391.2}) + 4.1 \times 10^{36} \left[\frac{M(^{44}\mathrm{Ti})}{10^{-4}\, M_\odot}\right] e^{-t/28489.5} \text{ ergs s}^{-1} , \tag{5}$$

assuming 0.07 $M_\odot$ of ^{56}Ni and ^{57}Ni/^{56}Ni is 1.5 times the solar ^{57}Fe/^{56}Fe ratio, or 2.5×10^{-3} $M_\odot$. The [O II] λλ3726, 3728 flux is then estimated to be

$$F_{[\mathrm{O\,II}]} = 5.5 \times 10^{-10} \eta D_\gamma \left(\frac{L_\gamma}{9.1 \times 10^{41} \text{ ergs s}^{-1}}\right) \times \left(\frac{v}{2000 \text{ km s}^{-1}}\right)^{-2} \left(\frac{t}{2000 \text{ days}}\right)^{-2} \left(\frac{M_O}{M_\odot}\right) \times \left(\frac{D}{50 \text{ kpc}}\right)^{-2} \text{ ergs cm}^{-2} \text{ s}^{-1} , \tag{6}$$

where D is the distance to the LMC, t is in units of days, and we have taken $\chi_{\mathrm{eff,O\,I}} = 26.7$ eV.

As a further test of our line identification, we need to estimate the amount of oxygen mass required to produce the [O II] λλ3726, 3728 doublet. The line fluxes after 1500 days are also very sensitive to the exact amount of energy input to the ejecta, a higher energy input can reduce the mass of oxygen required to reproduce the observed line flux. Woosley & Hoffman (1991) argue that the ^{44}Ti mass could range from 10^{-6} to 10^{-4} $M_\odot$. In a more recent calculation, Timmes et al. (1996) found an upper limit of $\sim 1.5 \times 10^{-4}$ $M_\odot$ of ^{44}Ti that can be synthesized in a Type II supernova like SN 1987A. Late-time observations show that although time-dependent effects (Fransson & Kozma 1993) can reduce the amount of energy sources required to fit the bolometric light curve, some additional energy source such as an accreting X-ray pulsar and/or a pulsar are still necessary to fit the observations (Bouchet et al. 1994).

The observed [O II] λλ3726, 3728 flux corrected by interstellar extinction on day 1862 is $8.6 \pm 1.6 \times 10^{-14}$ ergs cm^{-2} s^{-1}, and on day 2210 it is $7.1 \pm 1.4 \times 10^{-14}$ ergs cm^{-2} s^{-1}. These numbers are reasonably reproduced by assuming a ^{44} Ti mass of 4×10^{-4} $M_\odot$ and still keeping the mass of oxygen in a range that is consistent with that obtained by Fransson, Houck, & Kozma (1994). We found from equations (5) and (6),

$$\eta D_\gamma M_{\rm O}(v/2000 \text{ km s}^{-1})^{-2} = 5.1\ M_\odot \qquad (7a)$$

for the 1992 observation and

$$\eta D_\gamma M_{\rm O}(v/2000 \text{ km s}^{-1})^{-2} = 7.6\ M_\odot \qquad (7b)$$

for the 1993 observation, respectively. In a simple type of analysis similar to the above, Fransson et al. (1994) derive a lower limit of $M_{\rm O} \geq 3(v/1500 \text{ km s}^{-1})^2\ M_\odot$. If we assume, as derived by Kozma & Fransson (1992), that $D_\gamma \leq 3$, we then obtain, for typical velocities of the oxygen shell around 1500 km s^{-1}, a lower limit for the oxygen mass of $\eta M_{\rm O} \geq 0.96(v/1500 \text{ km s}^{-1})^2\ M_\odot$. The correction for collisional excitation requires knowledge of the electron density, which depends further on the clumpiness and ionization fraction of the ejecta. To be consistent with Fransson et al. (1994), we require η to be around 0.3, which can be achieved if the electron density is about 8.4×10^3 cm^{-3}. The corresponding ionization fraction is $2.8 \times 10^{-3} f_{\rm O}$ for 3 $M_\odot$ of oxygen distributed inside a sphere with maximum velocity 1500 km s^{-1}, where $f_{\rm O}$ is the volume-filling factor of the ejecta. It should be noted that the oxygen masses derived in the simplified approach of Fransson et al. (1994) are larger than the 1.2–1.5 $M_\odot$ derived from the [O I] λλ6300, 6364 lines by Li & McCray (1992) and Chugai (1994). In their more detailed models, a lower limit of oxygen mass of 1.5 $M_\odot$ was derived. The oxygen mass derived by Fransson et al. (1994) is also larger than or close to the upper limit of the 0.24–1.6 $M_\odot$ predicted by explosion models of the SN 1987A progenitor (Hashimoto, Nomoto, & Shigeyama 1989; Woosley 1988; Thielemann, Nomoto, & Hashimoto 1996). It remains to be seen if a revised analysis of both the line fluxes and profiles of the earlier [O I] λλ6300, 6364 data will bring these numbers into agreement. However, it is encouraging that the order of oxygen mass required to produce the fluxes of the [O II] λλ3726, 3728 line is correct even in this simple analysis.

The [O II] λλ3726, 3728 line can also be used to put a limit on the electron density in the oxygen-rich region. One approach is to solve the ionization equilibrium time dependently, in a way similar to that for the [O I] λλ6300, 6364 line described by Fransson et al. (1994). The line strengths and profiles set constraints on both the oxygen mass and its geometrical distribution. We outline here a simpler method for obtaining the electron density. Because of the freeze-out effect, the total number of recombinations per unit time will be larger than the total number of ionizations. An upper limit for the [O II] λλ3726, 3728 luminosity is obtained by assuming that each ionization to the excited states of O^+ decays only via the radiative process:

$$\xi h\nu \alpha_{\rm O^+} N_{\rm O\,II} N_e / f_{\rm O}^2 V \geq L_{[\rm O\,II]\,\lambda 3727}\,, \qquad (8)$$

where ν is the frequency of the transition, $\alpha_{\rm O^+}$ is the recombination coefficient of O^+, which equals $3.201 \times 10^{-13} T_4^{-0.688}/(1 - 0.0174 T_4^{1.707})$ with T_4 being the temperature in units of 10^4 K (Arnaud & Rothenflug 1985), and V is the volume of the emitting region. Taking the observed fluxes for $L_{[\rm O\,III]\,\lambda 3727}$, it is easy to derive from equation (8) that

$$\langle N_{\rm O\,II} N_e \rangle^{1/2} \geq 5400 f_{\rm O}^{-1} \left(\frac{v}{2000 \text{ km s}^{-1}}\right)^{-3/2} \times \left(\frac{t}{2000 \text{ days}}\right)^{-3/2} \text{cm}^{-3}\,. \qquad (9)$$

If we assume that mixing in the ejecta is macroscopic, equation (9) then gives approximate values of the average electron density in oxygen-rich regions of the ejecta. The corresponding recombination timescale of the oxygen-rich regions is then about 849 days, which is longer than the radioactive timescale but smaller than the dynamical timescale. This confirms that time-dependent effects (Kozma & Fransson 1993) are important at the epoch of these observations.

The most useful aspect of the identification of the [O II] λλ3726, 3728 line is that it provides an interesting method to estimate the amount of energy powering the ejecta. According to the mechanism outlined above, the [O II] λλ3726, 3728 line is powered mainly by ionization followed immediately by excitations; because the spontaneous decay timescale of the excited level is only a few hours, much shorter than the radioactive timescale or the dynamical timescale, the time-dependent effects as studied by Kozma & Fransson (1993) will never be important for the late-time evolution of the [O II] λλ3726, 3728 lines. The [O II] λλ3726, 3728 line strengths should therefore provide a reliable measure of the energy sources powering the late-time emission from supernova ejecta that is immune to time-dependent effects. Here we have derived an equivalent of about 4×10^{-4} $M_\odot$ of ^{44}Ti to power the late-time spectra. The method may be complicated by blending with iron lines near 3727 Å (Chugai et al. 1996), in which case it will provide an upper limit to the total amount of the underlying energy sources.

3.3. *Magnesium*

There are four magnesium lines observed in the spectrum. In addition to the semiforbidden Mg I] λ4571 line in the optical, the resonance lines Mg I λ2852 and Mg II λλ2795, 2802 are the strongest emission features in the ultraviolet. The most remarkable feature of the magnesium lines is the apparent difference of the line width in the ultraviolet and in the optical. Though it seems that all the lines show similar extended redshifted tails, the overall line profiles are much broader in the ultraviolet than in the optical. Notably, the

FWHM of the Mg I λ2852 line is more than twice the FWHM of the Mg I] λ4571 line and is broader than all of the optical lines. Because the Mg II λλ2795, 2802 lines are blended, and its red wing blended with the Mg I λ2852 line, it is impossible to deblend the lines and estimate their FWHM accurately. It is, however, very likely that the widths of the Mg II λλ2795, 2802 lines are comparable with that of the Mg I λ2852. The line profiles at the rest wavelength of Mg I λ2852 at different epochs are shown in Figure 6, together with the Hα lines for comparison.

The difference in line width offers a straightforward explanation for the size difference of the SN 1987A ejecta in the optical and UV, as measured from the *HST* direct images obtained with FOC. Jakobsen et al. (1994) showed that the SN 1987A ejecta are resolved by the *HST*. The measured size in the ultraviolet is twice that in the optical. Since the strongest optical lines are from decays of metastable levels that are optically thin, and the central wavelength for the UV image is at 2700 Å, which is close to the resonance lines of magnesium in the ultraviolet, the observed differences in the emission line width are clearly due to the fact that the UV lines are formed at higher velocity further out in the ejecta. This gives a natural explanation of the observed size for the ejecta. A detailed analysis of the ultraviolet and optical images is an interesting problem that we will defer to a separate study.

3.4. *Iron Lines and Line Blending*

Numerous iron lines are present in the late-time spectra of SN 1987A, although reliable identifications of these lines are difficult because the widths of the lines are so large that all the iron lines are strongly blended. However, in the ultraviolet, the Fe II emission lines from multiplets UV 1 and UV 2 are conspicuously strong. Iron probably makes a major contribution to the diffuse emission complex at wavelengths from 3000 Å to 3850 Å; for instance, the Fe II optical multiplets 1, 2, 3, 4, 5, 6, 7, 16, and 29 can be the major contributors. Fe I lines from optical multiplets 4, 5, 6, 20, 21, 23, 24, and 25 may also be significant in SN 1987A; they are observed to be strong in the wavelength range from 3500 Å to 3900 Å in the narrow-line quasar PHL 1092 (Bergeron & Kunth 1980) and in the Seyfert galaxy I Zw 1 (Oke & Lauer 1979). Note that the Balmer continuum and the [O II] λ3727 Å line lie just above this diffuse emission complex. The iron lines may affect the line profiles and intensities of the Balmer continuum and of [O II] λλ3726, 3728. Quantitative estimates of this effect require rigorous models of the iron emission which are difficult and uncertain. In our analysis of the Balmer continuum (§ 3.1.2) and the [O II] λλ3726, 3728 line (§ 3.2.2), we have assumed that the iron lines from 3500 Å to 3900 Å are strongly blended and can be approximated by a smooth curve. This approximation is perhaps not too far from reality considering the fact that most of the Fe I and Fe II lines may be optically thick and severely blended. The emission feature from 4180 to 4515 Å shows three distinct peaks. Emission lines in the same wavelength range exist also in I Zw 1 and are identified with [Fe II] lines (Oke & Lauer 1979). Some major contributors to these lines are [Fe II] λ4244 (21 F), [Fe II] λ4287 (7F), [Fe II] λ4320 (21 F), and [Fe II] λ4458 (6F).

The profile of Mg I λ2852 may also be affected by iron lines. However, the *HST* direct images show strong evidence that the size of the ejecta in the UV filter F275W is larger than that in the optical (§ 3.3; Jakobsen et al. 1994). The Mg II λλ2795, 2802 and Mg I λ2852 lines contribute about 35% to the total integrated light in the F275W filter. The ejecta size in the direct UV images can be understood with an intrinsically broader profile of the lines without strong iron contamination.

3.5. *Asymmetries*

The highest detectable expansion velocities are given in Table 4 for the strongest lines. They are all measured on the redshifted side of the profiles. The lines that show the fastest expansion are the Hα and Mg I λ2852 lines, with velocities up to 10,000 km s^{-1}. Such a high velocity for Mg I λ2852

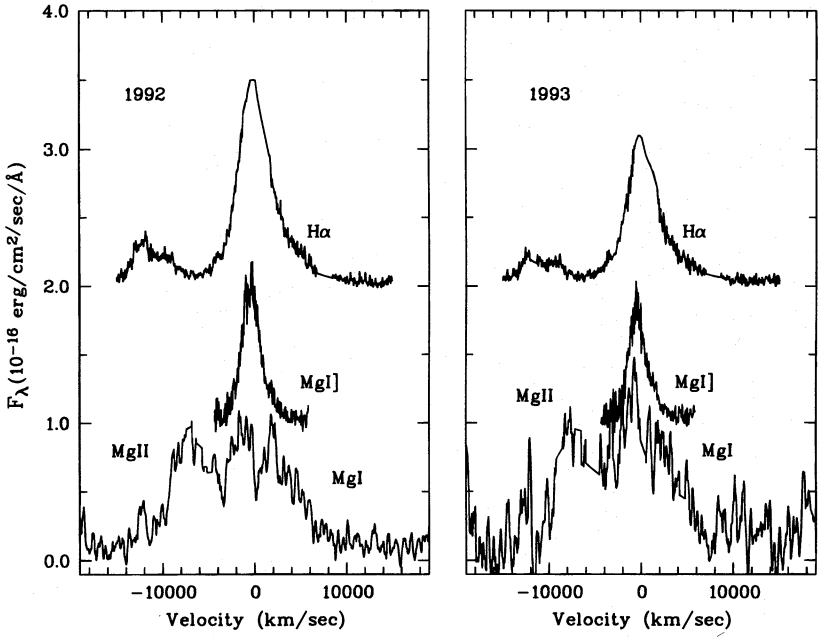

FIG. 6.—The Mg I λ2852 line is compared with the Hα and Mg I] λ4571 lines. From top to bottom, the profiles are Hα, Mg I] λ4571, and Mg I λ2852. Both the Mg I λ2852 and Hα lines show high-velocity components reaching 10,000 km s^{-1}, but the FWHM of the Mg I λ2852 line is much larger than that of any other observed lines.

TABLE 4

MAXIMUM OBSERVABLE VELOCITIES FOR STRONG LINES

Line	1992 Mar (km s^{-1})	1993 Mar (km s^{-1})
Hα	11000	11500
Hβ	7200	6900
[O I] λ6300	6000	5800
Mg I] λ4571	4000	3900
[O II] λλ3726, 3728	4400	4750
Mg I λ2852	10000	10000
Balmer Continuum	3100	2700

indicates clearly that a significant amount of the line flux is produced in the receding side of the hydrogen envelope of the ejecta.

Comparisons between the line profiles of Hα, Hβ, Mg I] λ4571, [O I] λλ6300, 6364, and [O II] λλ3726, 3728 show strong similarities. They are all blueshifted by a similar amount and exhibit extended redshifted wings. The blueshifts of the line peaks with respect to the narrow nebular lines vary from 300 to 500 km s^{-1}. Considering the uncertainties in the measurements and the lack of clear measurable peaks for many lines, these numbers are about the same as those reported earlier from ground-based studies that show that the peaks are blueshifted by about 800 and 500 km s^{-1} for Mg I] λ4571 and [O I] λ6300 (Bouchet et al. 1993) on around day 2000.

It has been convincingly shown that the blueshift of the emission lines is due to dust formation in the SN 1987A ejecta (Lucy et al. 1989). Lucy et al. (1991) show evidences of a two-component structure of the dust, diffuse small grains that produce the selective extinction at short wavelength, and very dense dust clumps that give rise to the wavelength-independent effect. By the time of these observations, the ejecta had expanded several times, and its density was so low that the diffuse component as studied by Lucy et al. (1989, 1991) were optically thin. Applying the models of the line profiles of Lucy et al. (1989), we find that the optical depth required to account for the blueshifts in the current data is practically the same as in early measurements by Lucy et al. (1989, 1991). This property for the extinction can be explained only if most of the dust that condensed in the SN 1987A ejecta is distributed in dense clumps whose optical depth remains far above unity even at this late stage of evolution. Assuming that the dust clumps expand homologously, the optical depth then scales as $\sim t^{-2}$, and a lower limit for the optical depth of each individual dust clump on day 500 after explosion must be above 16. By requiring the dust blobs to be optically thick, we can derive a lower limit to the total mass of dust in the supernova ejecta as

$$M_{\rm dust} \geq 1.78 \times 10^{-5}\, M_{\odot} \left(\frac{\tau}{0.4}\right)\left(\frac{\tau_b}{1}\right)\left(\frac{a}{0.1\ \mu{\rm m}}\right) \times \left(\frac{v}{2000\ {\rm km\ s^{-1}}}\right)^2 \left(\frac{\rho_d}{1\ {\rm g\ cm^{-3}}}\right), \quad (10)$$

where τ is the effective optical depth of the dust blobs, τ_b is the optical depth of each individual dust blob, a is the radius of the dust particles, and ρ_d is the density of the dust grains.

Inspection of Figures 5*a*, 5*b*, and 6 showed a weak but definite wavelength-dependent effect of the extinction, especially for the lines Mg I] 4571 Å, [O I] 6300 Å, and Hα. In their analysis of observations collected at around day 550, Lucy et al. (1991) attributed this wavelength dependence as produced by the selective extinction of the diffuse dust component. At around day 2000, this diffuse component should have become optically thin and ineffective in affecting the line profiles. This may imply that dust formation continued even at the late stage or that the dense dust clumps were only partially optically thick at around day 2000.

The origin of the red wing in each line profile is most likely to be the relic of the asymmetries observed in a much earlier phase, as shown by Phillips & Heathecote (1989) and Hanuschik & Dachs (1987) for the Hα line and most clearly by Larson et al. (1987) for Paα. Because the supernova is now powered mainly by the decay of ^{57}Co and ^{44}Ti, it thus seems that ^{57}Co and ^{44}Ti are also asymmetrically distributed, in a way quite similar to that of ^{56}Co.

4. CONCLUSIONS

We have analyzed the *HST* spectra of the ejecta of SN 1987A. The optical spectra of SN 1987A resemble strongly those of novae many decades after explosion (Williams 1992). This should not be surprising, considering the fact that the temperatures of both the SN 1987A ejecta and the nova shells are comparable. The hydrogen Balmer continuum yields accurate estimates of electron temperature in the SN 1987A ejecta. The derived temperatures of the hydrogen emitting region are 500 K and 400 K on days 1862 and 2210, respectively. Such low temperatures are consistent with model calculations of Kozma & Fransson (1993) and Fransson & Kozma (1994).

The [O I] λλ6300, 6364 doublet is decomposed into separate [O I] λλ6300 and 6364 lines assuming they have an identical profile and an intensity ratio of 3:1. The decomposed [O I] profile is broadly consistent with the profiles of other lines such as Mg I] λ4571, [O II] λλ3726, 3728, and even the hydrogen Balmer lines. The line ratios $R = F$([O I] λ6300)/F([O I] λ6364) cannot be estimated accurately without knowing the true [O I] λ6300 line profile. Early model calculations of the oxygen mass that used the doublet ratio R derived on the basis of line profile fitting or line peak measurements are subject to this uncertainty. A robust analysis of the [O I] λλ6300, 6364 doublet using the mechanism proposed by Chugai (1988, 1994) can be obtained only by data analysis that makes a careful assessment of the line strengths without assuming a particular shape for the line profile. This needs to be applied uniformly to both early and late data.

We found that the [O II] λλ3726, 3728 line has become surprisingly strong in the SN 1987A ejecta. The [O II] λλ3726, 3728 doublet strength is modeled by considering collisional ionizations of neutral oxygen directly to excited states of O^+. We note that the [O II] λλ3726, 3728 line potentially gives an estimate of the oxygen mass. Our simple analysis sets a lower limit for the SN 1987A oxygen mass as shown by equation (8). The mechanism responsible for the [O II] λλ3726, 3728 doublet is not unique to SN 1987A but may be applicable to other supernovae as well. Moreover, the mechanism is not unique to atomic oxygen but may also apply to other abundant elements such as C and Ne. If this interpretation is correct, the [O II] λλ3726, 3728 doublet will to be an interesting measure of the energy sources powering late-time emission of the supernova, independent of time-dependent recombination.

The Mg I λ2852 and Mg II $\lambda\lambda$2795, 2802 lines in the ultraviolet form at high velocity and large radius and thus provide a straightforward explanation for the size difference of the SN 1987A ejecta in the ultraviolet and in the optical as deduced from the *HST* direct images (Jakobsen et al. 1993, 1994).

The ensemble of optical emission lines is blueshifted by an amount comparable to those reported earlier (Lucy et al. 1989, 1991), which requires continued high optical depth in dust from day 500 to 2000. A lower limit to the dust mass in the SN 1987A ejecta was derived as shown in equation (10). The line profiles are asymmetric; redshifted tails are observed for all the lines, up to 10,000 km s^{-1} for Hα and Mg I λ2852. The asymmetric tails are perhaps relics of the asymmetries observed at much earlier phases (Hanuschik & Dachs 1987; Larson et al. 1987; Phillips & Heathecote 1989), thus implying that ^{57}Co and ^{44}Ti, just like ^{56}Co, are distributed asymmetrically.

Future observations using *HST* should prove to be important in studying the evolution of the SN 1987A ejecta. Luo, McCray, & Slavin (1994) predict that the expanding ejecta of SN 1987A will hit the circumstellar ring in 1999 ± 3; a recent model by Chevalier & Dwarkadas (1995) shows that the interaction may start in 2005 ± 3. When the interaction begins, the supernova will become a bright ultraviolet source again. The *HST* data provide unique wavelength coverage and spatial resolution and produce a large number of line fluxes that can be combined with models to extract a clearer picture of both the ejecta and the circumstellar ring.

This research is supported in part by NASA grant GO 5652, NAGW 2905, and NSF grant 9218035. We are grateful for conversations with R. Chevalier, N. Chugai, A. M. Khokhlov, B. Leibundgut, J. Spyromilio, E. J. Wampler, B. Wills, and S. E. Woosley.

REFERENCES

Arnaud, M., & Rothenflug, R. 1985, A&A S, 60, 425
Bergeron, J., & Kunth, D. 1980, A&A, 85, L11
Bouchet, P., Danziger, I. J., Gouiffes, C., Della Valle, M., & Moneti, E. 1994, in IAU Colloq. 145, Supernovae and Supernova Remnants, ed. R. McCray & Z.-R. Wang (Cambridge: Cambridge Univ. Press), in press
Chevalier, R. A., & Dwarkadas, V. V. 1995, ApJ, 452, L45
Chugai, N. N. 1988, Astron. Tsirk., 1525
———. 1991a, Soviet Astron., 35, 171
———. 1991b, Soviet Astron. Lett., 17, 400
———. 1994, ApJ, 428, L17
Chugai, N. N., Danziger, I. J., Wampler, E. J., & Wang, L. 1993, unpublished
Chugai, N. N., et al. 1996, ApJ, submitted
Clayton, D. C., Leising, M. D., & The, L.-S. 1992, ApJ, 399, L141
Fransson, C., Casatella, A., Gilmozzi, R., Kirshner, R. P., & Panagia, N. 1989, ApJ, 336, 429
Fransson, C., & Chevalier, R. A. 1989, ApJ, 343, 323
Fransson, C., Houck, J., & Kozma, C. 1994, in IAU Colloq. 145, Supernovae and Supernova Remnants, ed. R. McCray & Z.-R. Wang (Cambridge: Cambridge Univ. Press), in press
Fransson, C., & Kozma, C. 1993, ApJ, 408, L25
Hanuschik, R., & Dachs, J. 1987, A&A, 182, L29
Hashimoto, M., Nomoto, K., & Shigeyama, T. 1989, A&A, 210, L5
Jakobsen, P., Jedrzejewski, R., Macchetto, F., & Panagia, N. 1994, 435, ApJ, L47
Jakobsen, P., Macchetto, F., & Panagia, N. 1993, ApJ, 403, 736
Kirshner, R. P., Sonneborn, G., Grenshaw, D. M., & Nassiopoulos, G. E. 1987, ApJ, 320, 602
Kozma, C., & Fransson, C. 1992, ApJ, 390, 602
Laher, R. R., & Gilmore, F. R. 1989, J. Phys. Chem. Ref. Data, 19, 277
Larson, H. P., Drapatz, S., Mumma, M. J., & Weaver, H. A. 1987, in ESO Workshop on the SN 1987A, ed. I. J. Danziger (Garching: ESO), 147
Li, H., & McCray, R. 1992, ApJ, 387, 309
———. 1995, ApJ, 441, 821
Lucy, L. B., Danziger, I. J., Gouiffes, C., & Bouchet, P. 1989, in IAU Colloq. 120, Structure and Dynamics of the Interstellar Medium, ed. G. Tenorio-Tagle, M. Moles, & J. Melnick (New York: Springer), 164
Lucy, L. B., Danziger, I. J., Gouiffes, C., & Bouchet, P. 1991, in Supernovae, ed. S. E. Woosley (New York: Springer), 82
McCray, R. 1993, ARA&A, 31, 175
Luo, D., McCray, R., & Slavin, J. 1994, ApJ, 430, 246
Oke, J. B., & Lauer, T. R. 1979, ApJ, 230, 360
Osterbrock, D. E. 1989, Astrophysics of Gaseous Nebulae and Active Galactic Nuclei (Mill Valley: University Science)
Panagia, N., Gilmozzi, R., Clavel, J., Barylak, M., Gonzales Riesta, R., Lloyd, C., Sanz Fernandez de Cordoba, L., & Wamsteker, W. 1987, A&A, 177, L25
Panagia, N., Scuderi, S., Gilmozzi, R., Challis, P. M., Garnavich, P. M., & Kirshner, R. P. 1996, ApJ, 459, L17
Péquignot, D., Petitjean, P., & Boisson, C. 1991, A&A, 251, 680
Phillips, M. M., & Heathecote, S. R. 1989, PASP, 101, 137
Phillips, M. M., & Williams, R. E. 1991, in Supernovae, ed. S. E. Woosley (New York: Springer), 36
Plait, P. C., Lundqvist, P., Chevalier, R. A., & Kirshner, R. P. 1995, ApJ, 439, 730
Pun, C. S. J., et al. 1995, ApJS, 99, 223
———. 1996, in preparation
Spyromilio, J., Meikle, W. P. S., & Allen, D. A. 1990, MNRAS, 242, 669
Spyromilio, J., & Pinto, P. A. 1991, in Proc. ESO/EIPC Supernovae Workshop, ed. I. J. Danziger (Garching: ESO), 423
Swartz, D. 1991, in Supernovae, ed. S. E. Woosley (New York: Springer), 434
Thielemann, F. K., Nomoto, K., & Hashimoto, M. 1996, ApJ, 460, 400
Timmes, F. X., Woosley, S. E., Hartmann, D. H, & Hoffman, R. D. 1996, ApJ, 464, 332
Walborn, N. R., Phillips, M. M., Walker, A. R., & Elias, J. H. 1993, PASP, 105, 1240
Wampler, E. J., & Richichi, A. 1989, A&A, 217, 31
Wang, L., D'Odorico, S., Gouiffes, C., & Wampler, E. J. 1992, IAU Circ. 5449
Williams, R. E. 1982, ApJ, 261, 170
Woosley, S. E. 1988, ApJ, 330, 218
Woosley, S. E., & Hoffman, R. D. 1991, ApJ, 368, L31
Xu, Y., & McCray, R. 1991, ApJ, 375, 190